Modeling Analysis of Methane Catalytic Partial Oxidation as a Route to Produce Hydrogen Rich Mixtures

Jorge E. P. Navalho, José M. C. Pereira and José C. F. Pereira
LASEF
Instituto Superior Técnico, Universidade Técnica de Lisboa,
Av. Rovisco Pais 1, 1049-001 Lisboa, Portugal
email: jorge.navalho@ist.utl.pt   http://www.lasef.ist.utl.pt

Abstract

The present communication intends to report the numerical activities carried out to the development of a catalytic partial oxidation of hydrocarbons based reformer. A series of numerical simulations were performed with a numerical model which considers the coupling between surface chemistry and heat and mass transport phenomena taking place at both bulk gas phase and catalytic porous layer.

A procedure to assess about an optimal range for operating conditions is developed based on both fuel conversion and reformer efficiency achieved at catalyst's outlet section. The catalyst surface temperature is also monitored to guarantee a stable operation far from the thermal catalyst deactivation regime. An optimal range for air ratio, fuel flow rate and an inlet reformer temperature are pointed out for two case studies: the first case involves the performance of a nonadiabatic reformer and the second case considers an adiabatic reactor by adding to the nonadiabatic reformer disposal an inert front heat shield. The comparison between the performance of both reactors shows that heat losses from nonadiabatic reactor cause severe injuries on fuel conversion and reformer efficiency especially for low fuel flow rates. Consequently, the most favorable operating conditions achieved with the nonadiabatic reformer are attained at high flow rates.

Keywords: Catalytic Partial Oxidation, Methane, Synthesis Gas, Fuel Conversion, Reformer Efficiency.

1   INTRODUCTION

Catalytic partial oxidation (CPOx) of hydrocarbons as a route to produce synthesis gas (a mixture of H_2 and CO) has received an increasing attention from the beginning of the 90's of the last century after Schmidt and co-workers [1-2] reported excellent fuel conversion and synthesis gas selectivity under autothermal and short contact time conditions using rhodium and platinum noble metals over monoliths. However, the first papers dealing with catalytic partial oxidation are dated of late 20's to 40's of the same century [3-5] but at the time this process revealed some disappointing features such as the strong tendency to coke deposition on Ni catalysts, leading to its fast deactivation which was not studied in detail, and the huge inlet feed temperature required to achieve high selectivity of syngas. This poor knowledge combined with the success of steam reforming was responsible for the decaying attention for decades on this process [6].

In fact, this process has several advantages over other well established technologies to produce syngas like the energy intensive steam reforming technology. The catalytic partial oxidation of hydrocarbons is globally described by the following reaction:

$$C_xH_y + \frac{x}{2}O_2 \longrightarrow xCO + \frac{y}{2}H_2, \ \Delta H^\circ{}_R < 0$$

In the case of being methane the fuel on the above reaction, the partial oxidation is mildly exothermic with a heat of reaction at standard conditions of about $-36kJ/mol$ and with H_2/CO ratio of 2 which is optimal for downstream chemical processes (methanol or Fischer-Tropsch synthesis). Besides more economical than methane steam reforming, which globally is a strongly endothermic reaction ($\Delta H_R^\circ = +206kJ/mol$), this technology also requires much simpler equipment, shorter residence times (millisecond contact times) and presents the possibility to scale down (or up) [7] the reformer for a specific application, resulting in small reactors with a fast dynamic response due to its low heat capacity being suitable for mobile or stationary decentralized applications [8]. Since natural gas has a high dissemination in the industrialized countries, catalytic partial oxidation offers a promising way to produce H_2 rich mixtures for domestic applications namely to feed fuel cells for electrical generation purposes at residential level. Heat generation from thermal recovery of the fuel cell exhaust gases is also an opportunity to increase even more the overall efficiency of the primary energy

utilization into final energy. Indeed, combined decentralized production of heat and power can reduce the energy distribution losses [9]. Moreover, since methane can be produced during anaerobic decomposition of organic waste (resulting in an energy gas carrier currently known as biogas), the usage of methane coming from this origin, through CPOx reactors, also contributes to a more sustainable and carbon neutral world. Apart from being a feedstock for synthesis of chemical compounds and to act as a fuel preprocessor for fuel cells, CPOx of hydrocarbons have also found applications on flame stabilization in gas turbines operating with lean conditions [8].

The European FC-District project, which aims to develop and build a decentralized μ-CHP system by tailoring each one of its components, is the main motivation for all numerical activities herein reported. The μ-CHP system is composed mainly by a Solid Oxide Fuel Cell (SOFC), a CPOx reformer, a desulfurizer unit to remove traces of sulfur components in the feed stream before entering in the catalytic reformer, a fuel mixer, a off-gas burner to remove toxic gases such as CO and to extract the energy content of the exhaust anode fuel cell gas and several heat exchangers, despite all the remaining electrical and electronic components. A SOFC shows several advantages over the remaining types of fuel cells due to its tolerance of CO and other minor impurities in the feed stream (syngas), its range of operating temperatures (600 to 1000ºC) and its high energy content exhaust gas for heat generation purposes [10]. A SOFC combined with a post-combustion in lean or ultra-lean conditions of the remaining H_2 and CO mixtures increases the overall combined system efficiency up to 90% [11].

2   CHARACTERIZATION OF ACTUAL CPOX REACTOR

CPOx reformer applied in the FC-District project has to fulfill two main requirements: high total reformer efficiency and low pressure drop. A commercial ceramic honeycomb monolith washcoated with Platinum Group Metals (PGMs) catalysts was employed without using radiative heat shields upstream or downstream to the catalytic region. Several reformer prototypes have been investigated experimentally by TUBAF [12] and numerical results are concerned with experimental data considering the geometrical properties of the monolith catalyst listed in Table 1.

Table 1 – Geometrical properties of the catalytic monolith provided by catalyst supplier.
*After washcoat application.

Cell density [CPSI]	600	Porosity* [%]	70.0
Cell shape	Square	Specific surface area* [cm^{-1}]	32.27
Monolith diameter [cm]	3.7	Cell hydraulic diameter* [cm]	0.087
Monolith length [cm]	3.0	Washcoat thickness [μm]	40

Moreover, the reformer performance was experimental and numerically characterized under the operation of several fuel compositions but the present report only covers modeling analysis with pure methane.

Figure 1 depicts the reactor configuration as well as the main chemical species engaged in its application. In the present situation the feed gas stream is composed only by methane and air but in the range of fuel applicability to the FC-District CPOX reactor, biogas and a mixture of methane and propane or nitrogen have also been considered. Except for biogas utilization, the characterization of the reformer performance under the operation of the remaining fuels is due to the different natural gas composition over the European countries.
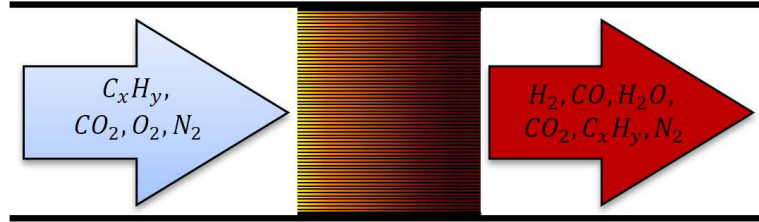
Figure 1 - Reactor configuration and the main composition of the reacting mixture at inlet and outlet manifolds.

Table 2 presents the relevant thermo-physical properties of the reactor for modeling purposes. Since the present study regards only analysis in steady-state conditions, values for specific heat and density of the monolith are not useful in the applied mathematical model.

Table 2 – Thermo-physical properties of the CPOx reactor.

Solid conductivity [$W/(m.K)$]	3.0
Solid emissivity [-]	0.7
Washcoat density [kg/m^3]	1.5

3 GOVERNING EQUATIONS

Numerical modeling results herein reported were performed using a unidimensional heterogeneous mathematical model for a single channel of a fixed bed reactor. The model assumes no heat and mass transfer across channel walls, which is a quite good assumption when the incoming feed gas stream has constant properties (velocity, temperature and mixture composition) at the monolith entrance section and when all channels have the same thermal properties and equal catalytic distribution and activity. Fulfilling these conditions, all channels behave essentially alike and consequently just a single channel of the whole reactor is evaluated.

Being heterogeneous, the model includes phenomena taking place at two different phases: the bulk gas phase and solid phase (reactor walls). For each phase species mass balances and energy balance are performed and therefore the model is able to predict temperature profiles and product distribution for both phases along the axial direction of the channel. Thus, solid catalyzed reactions are accounted for in the balances of solid phase. Both phases are necessarily coupled together through external heat and mass transport properties given by Nusselt and Sherwood correlations respectively, proper for the range of operating conditions simulated and the geometrical properties of the catalyst carrier.

3.1 Gas phase balance equations

Species mass balances (equation (1)) and energy (equation (2)) equations of gas phase share the same phenomena: they consider mass and heat convection (between both phases) and diffusion. Following several literature findings [13-15] it was not considered gas phase reactions in the model gas phase equations since at typical methane CPOx conditions (atmospheric pressure and millisecond contact times) the heterogeneous reactions contribution is much more important than the contribution from gas phase reactions. However, it is largely accepted that homogeneous reactions become important at higher pressures ($> 5bar$) [14, 16-17] or when fueling the reactor with higher hydrocarbons than methane there is also an important chemical path due to homogeneous chemistry [18-21].

$$\varepsilon \rho_g \frac{\partial Y_{k,g}}{\partial t} = -\varepsilon \rho_g u \frac{\partial Y_{k,g}}{\partial x} - \frac{\partial}{\partial x}\left(\varepsilon \rho_g Y_{k,g} V_{k,g}\right) - a_V \rho_g K_{mat,k}\left(Y_{k,g} - Y_{k,w}\right) \tag{1}$$

The correction velocity formalism was employed in equation (1) to ensure mass conservation through the axial direction of the channel.

$$\varepsilon \rho_g C_{p,g} \frac{\partial T_g}{\partial t} = -\varepsilon \rho_g u C_{p_g} \frac{\partial T_g}{\partial x} + \frac{\partial}{\partial x}\left(\varepsilon k_g \frac{\partial T_g}{\partial x}\right) - \varepsilon \rho_g \sum_{k=1}^{KK_{gas}} Y_{k,g} V_{k,g} C_{p,k} \frac{\partial T_g}{\partial x} - a_V h (T_g - T_s) \qquad (2)$$

The third term one RHS of equation (2) is usually negligible comparing to the remaining terms but it is included in order to retain coherence between the energy and species mass balances, due to the distortion imposed by molecular diffusion on the species mass balances.

Momentum balance equation was not implemented in the model scheme since the pressure drop along monolith length is usually considered as negligible [8, 22].

3.2 Solid phase balance equations

Solid phase species mass balances are given by equation (3) which include external mass transport (mass convection) and molecular production/consumption due to surface chemistry.

$$\epsilon \rho_g \frac{\partial Y_{k,w}}{\partial t} = a_V \rho_g K_{mat,k} (Y_{k,g} - Y_{k,w}) + \dot{\omega}_{k,w} M_k \qquad (3)$$

Mass balances are performed in the interface between the free bulk gas flow and the external washcoat surface area. Regarding energy balance (equation (4)) it includes the axial heat conduction, interphase heat transport and the net heat release form surface reactions.

$$(1 - \varepsilon)\rho_s C_{p_s} \frac{\partial T_s}{\partial t} = \frac{\partial}{\partial x}\left(k_{s,eff} \frac{\partial T_s}{\partial x}\right) + a_V h (T_g - T_s) - \sum_{k=1}^{KK,w} \dot{\omega}_{k,w} H_k \qquad (4)$$

Transport diffusion limitations along washcoat layer (intraphase diffusional resistances) are already included in the surface molecular production/depletion term ($\dot{\omega}_{k,w}$) with a particular washcoat model (see §4.2.2).

3.3 Boundary Conditions

The computational domain applied in numerical simulations for the actual reactor configuration (Figure 1) starts at the inlet section of the catalytic region to its outlet section and hence the computational domain has 3.0cm (Table 1). Danckwerts type of boundary conditions were applied to both gas phase balance equations, due to the relative importance of molecular and heat diffusion in gas phase at the beginning of the computational domain. A radiative boundary condition was applied to the energy balance equation of the solid phase. At the outlet of the domain, it was imposed to all dependent variables Neumann boundary conditions of zero flux.

Table 2 – Boundary conditions applied on governing equations for the actual reformer disposal.

		$x = 0.0cm$	$x = 3.0cm$
GAS PHASE BALANCE EQUATIONS	**Species Mass**	$Y_{k,g} - Y_{k,in} + \dfrac{Y_{k,g} V_{k,g}}{u} = 0$	$\dfrac{\partial Y_{k,g}}{\partial x} = 0$
	Energy	$\rho_g C_{p,g} u (T_g - T_{g,in}) - k_g \dfrac{\partial T_g}{\partial x} = 0$	$\dfrac{\partial T_g}{\partial x} = 0$
SOLID PHASE BALANCE EQUATION	**Energy**	$k_s \dfrac{\partial T_s}{\partial x} - \sigma \varepsilon_s (T_{g,in}^4 - T_s^4) = 0$	$\dfrac{\partial T_s}{\partial x} = 0$

4 MODELING ISSUES

4.1 Chemical Kinetics

Heterogeneously solid catalyzed reactions were evaluated with one global reaction mechanism suitable for methane catalytic partial oxidation over PGMs catalysts [23]. This mechanism has shown to be strongly adequate to the real catalyst formulation and activity applied in the reactor used in the project. The mechanism comprises 6 chemical species ($CH_4, O_2, CO_2, H_2O, H_2$ and CO) and it follows an indirect consecutive syngas production scheme [6], through which syngas is only produced after the oxidation of some fuel through steam reforming reaction with the remaining unoxidized fuel. Water-gas shift and its reverse as well as H_2 and CO consecutive oxidation reactions are also taken into account in the molecular kinetic scheme. Kinetic rate equations follow the Langmiur-Hinshelwood (LH) type and its kinetic parameters can be found elsewhere [23].

The species production/consumption term from surface kinetics, which appears in both balance equations of solid phase, are given by expression (5).

$$\dot{\omega}_{k,w} = \sum_{R=1}^{NR} \upsilon_{k,R}.q_R.\eta_R.\xi.\rho_{cat} \qquad (5)$$

4.2 Transport Phenomena

There is a strong coupling between surface chemistry and transport of heat and mass between both phases and even within the same phase. This is mainly due to the fact that reactant species must travel from the bulk gas phase, through external mass transport, to the external catalyst surface and then diffuse in the pore structure of the washcoat layer. Along the washcoat thickness reactant species undergo through heat and mass transfer limitations in series with surface chemical reactions. Thus, two kinds of transport phenomena are herein involved: external or interphase and internal or intraphase.

4.2.1 External transport

External transport couples both phases in terms of energy and species mass balances and since the model is unidimentional this must be accounted for through proper correlations, which return the coefficients for heat and mass convection. Therefore, it is of paramount importance to employ adequate Nusselt and Sherwood correlations to correctly model this type of transport phenomena. Since the honeycomb monolith has square shaped channels (Table 1) the following Nusselt correlation is widely applied in literature [24]:

$$Nu = 2.977 + [8.827(1000X^*)^{-0.545}]exp(-48.2X^*) \qquad (6)$$

where, $X^* = \frac{x - x_{in,cat}}{d_h Pe_T}$

Sherwood correlation is simply achieved by the application of Chilton-Colburn analogy.

4.2.2 Internal transport – Mass transfer resistance

The washcoat application on reactor walls requires the diffusion of reactant species through the porous nature of the washcoat layer until they reach the catalytic particles and undergo in chemical surface reactions. Therefore, mass and heat transport limitations along washcoat layer can be severe but normally the achieved net result is largely profitable than without using any washcoat layer [25].

Hence the reaction-diffusion problem along washcoat thickness should be overcome using a detailed or a simplified washcoat model. These models aim to quantify the concentration and thermal gradients along the washcoat layer and therefore they intend to evaluate the average molecular consumption/formation rates at each reactor position. In general, increasing the washcoat thickness keeping constant its pore size distribution the gradients become more pronounced and its utilization becomes more inefficient. Therefore, in practice there is a

compromise between the washcoat thickness and the performance requirements of the catalyst, since using much more catalyst for a specific range of operating conditions does not return a significant difference on fuel conversion and syngas selectivity.

In this work, isothermal washcoat layer is assumed along a simplified approach using generalized effectiveness factors since the kinetic expressions follow the LH type. Internal diffusional resistances were then applied to each oxidation reaction considering O_2 the reactant species with lower effective diffusivity and consequently the limiting one. For methane steam reforming reaction CH_4 was considered the limiting species. Thus for these reactions, Thiele moduli are given by expression (7) where k corresponds to the limiting species.

$$\phi_{k,R} = \frac{\delta_{cat} q_R(C_k^S) \xi \rho_{cat}}{\sqrt{2 \int_{C_k^{eq}}^{C_k^S} D_{eff,k} \, q_R(C_k) \xi \rho_{cat} dC}} \tag{7}$$

Finally, since the washcoat thickness is small it can be treated as a flat surface and therefore the effectiveness factor for each reaction is simply given by expression (8).

$$\eta_R = \frac{tanh(\phi_{k,R})}{\phi_{k,R}} \tag{8}$$

Effective diffusivities above required were computed using the random pore model [25] with a bimodal pore structure and with both molecular and Knudsen contributions through the Bonsaquet equation. A typical washcoat pore structure was assumed [27] and molecular diffusivities were evaluated using Füller-Schettler-Giddings correlation [28].

4.3 Numerical model

The above mathematical model was implemented in an in-house version of PREMIX code [28] from CHEMKIN family combustion softwares. Finite difference approximations are employed to reduce the boundary value problem to a system of nonlinear algebraic equations. Thus, convective and diffusion terms are discretized by central difference schemes and then, on a nonuniform coarse initial mesh, the program attempts to solve the problem by a damped Newton's method which determines a sequence of steps to achieve the true solution to all dependent variables. After the determination of the converged solution on a previous mesh, an adaptive mesh procedure is employed to reach finer meshes based on gradients and curvatures resolution between each grid point. Time-stepping procedure is also applied to achieve the steady state solution when the initial solution lies out of the steady state domain of convergence of Newton's method. More information about the numerical model herein employed can be found elsewhere [28-29].

All thermodynamic and transport data were evaluated using CHEMKIN libraries [30-31] with thermodynamic and transport coefficients given by GRI3.0 database [32]. This model was previously validated with excellent agreement against reference numerical and experimental data reported in literature [26].

5 RESULTS AND DISCUSSION

5.1 Model Validation

The comparison between experimental measurements and numerical simulations, for the actual reformer performance, are herein presented for 3 different working conditions. Therefore, Figure 2 presents gas and surface temperature profiles and integral product distribution in a dry basis. Numerical results are presented in solid or dashed lines whereas experimental measurements are presented by symbols.

As one can see the numerical results are in good agreement with experimental data. Moreover, the model has always shown a predictive behavior, with no adjustable parameters, for a large set of experimental measurements.
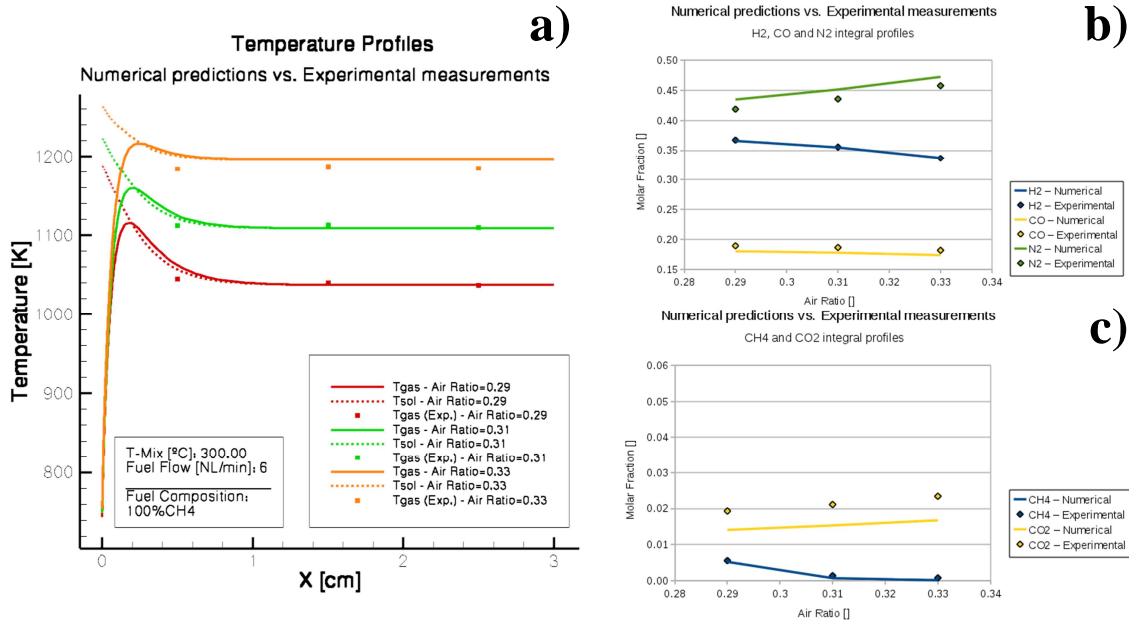
Figure 2 – Comparison between numerical simulation results and experimental data. a) Gas and solid temperature profiles; b), c) - Integral product distribuition in dry basis.

5.2 Optimal range for operating conditions

The main purpose of this section is to identify a range for air ratio (λ), fuel volumetric flow rate ($\dot{V}_{fuel}$) and an inlet reformer temperature (T_{mix}) that lead to higher levels of fuel conversion (X_{fuel}) and reformer efficiency (η_{ref}) along with a stable operation, ie. without deactivation issues, namely related with thermal deactivation mechanisms (sintering or phase transformations) [33]. It is broadly accepted for PGMs catalysts a maximum surface temperature ($T_{s,max}$) of about 1000ºC to guarantee a stable long term operation [22, 34]. Therefore, fuel conversion, reformer efficiency and surface maximum temperature are the control parameters herein employed to define an optimal range for operating conditions.

To accomplish the proposed goal, three inlet reformer temperatures were considered (250ºC, 300ºC and 350ºC), an air ratio range between 0.28 and 0.33 and a fuel volumetric flow rate range starting from 2 to 8 NL/min. This range of operating conditions has been considered suitable for CPOx reformer to assure a proper feed stream for SOFCs [12].

5.2.1 Actual reactor geometry

Since the catalytic layer starts at the beginning of the monolith reactor, a hot spot at the entrance section will appear due to the exothermic nature of the reactions in this region and consequently, radiative heat losses from the inlet section to the inlet manifold will decrease the temperature field inside the reactor and damage its performance. Starting with fuel conversion, Figure 3 shows that increasing the inlet reformer temperature the domain ($\lambda \times \dot{V}_{fuel}$) at which the fuel conversion exceeds 98% also increases. A fuel conversion equal or above to 98% will be taken into account to further define an optimal range for fuel flow rates and air ratios. As depicted in Figure 4, the reformer efficiency levels in the $\lambda \times \dot{V}_{fuel}$ domain also increase with inlet reformer temperatures. Hence, for the inlet reformer temperatures considered and in the $\lambda \times \dot{V}_{fuel}$ domain it was always found a maximum for reformer efficiency at 8NL/min but the corresponding air ratio decreased from 0.305, 0.30 and 0.29 for 250ºC, 300ºC and 350ºC, respectively. Moreover for 250ºC, 300ºC and 350ºC the maximum value for reformer efficiency is 87.1%, 87.9% and 88.7%, respectively.
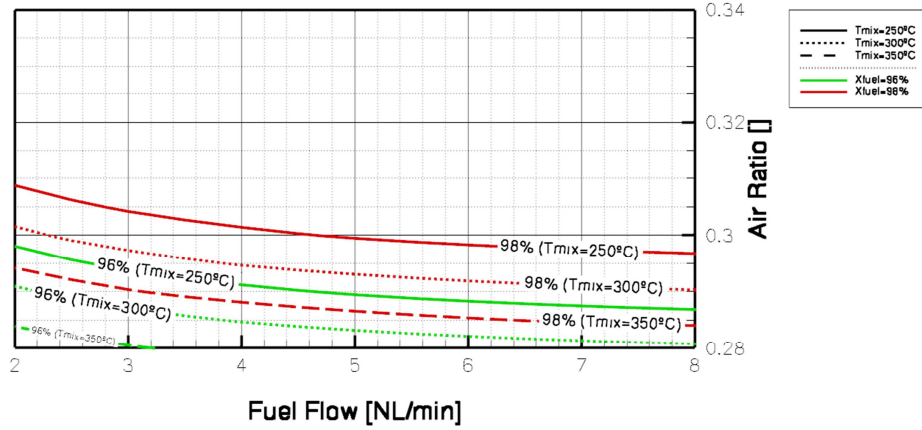
Figure 3 - Two isolines of fuel conversion (98% and 96%) for 3 different inlet reformer temperatures.

In fact, the variation observed on fuel conversion and reformer efficiency with fuel flow rate is largely due to the heat dispersion from the front section of the catalytic monolith. It is expected that the relative heat losses by radiation decrease with the input power, and consequently for low flow rates a worst performance is presumed when comparing it to the adiabatic reformer performance.
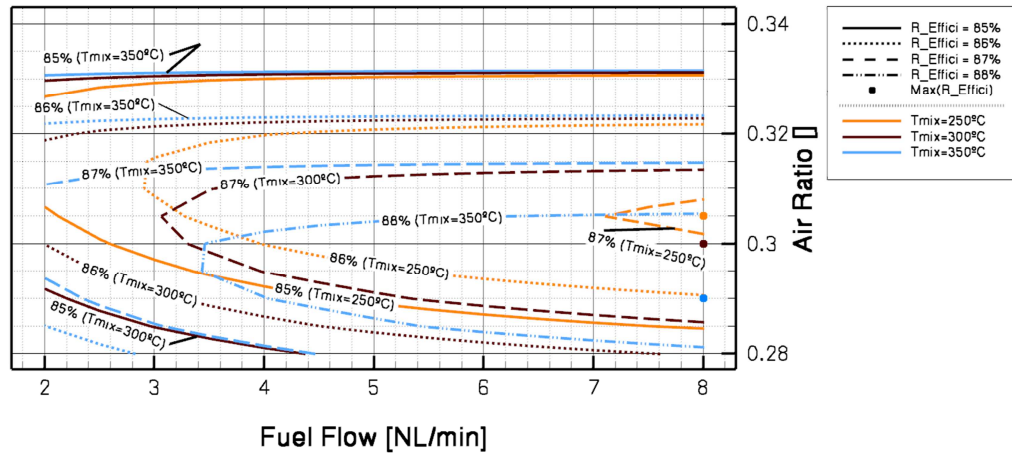

Figure 4 - Three/four reformer efficiency isolines for the three inlet reformer gas temperatures. The points at $\dot{V}_{fuel} = 8NL/min$ indicate, for each inlet gas temperature, the location of the maximum reformer efficiency.

In the absence of a specific requirement for the inlet reformer temperature, reformer efficiency equal or above 88% is herein chosen to define an optimal range for operating conditions and inherently an inlet reformer temperature of 350ºC is also selected. However, it is still need to guarantee an operating regime far from high surface temperatures and as expected the region of the domain which ensures a stable operation decreases when the inlet gas stream temperatures increases. Thereby, in Figure 5 one can define different ranges for air ratios and fuel flow rates for each inlet feed stream temperature that maximizes both fuel conversion and reformer efficiency and assures surface temperatures bellow the maximum allowed.

Finally, the optimal range for fuel flow rates and air ratios is defined by expression (9) and it is denoted in Figure 6 as "Optimal Operating Regime" for an inlet gas temperature of 350ºC.

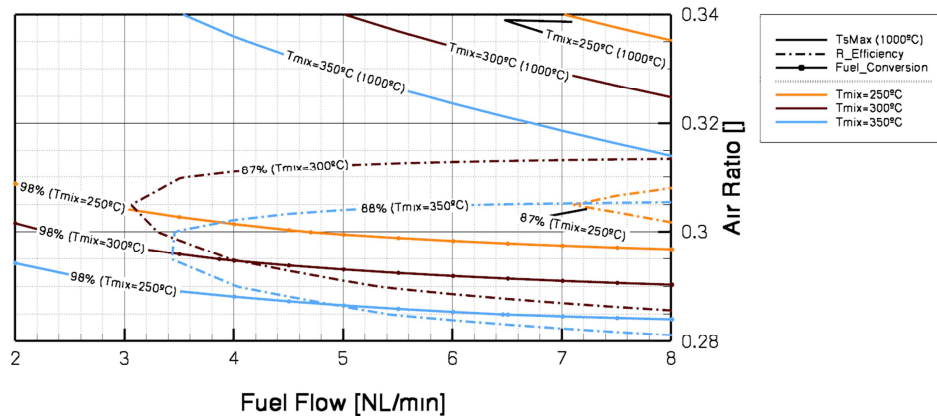$$\{X_{fuel} \geq 98\% \ \cap \eta_{ref} \geq 88\% \cap \ T_{s,Max} < 1000℃\} \tag{9}$$

Figure 5 - Isolines of fuel conversion, reformer efficiency and maximum allowable surface temperature for the actual reactor disposal.
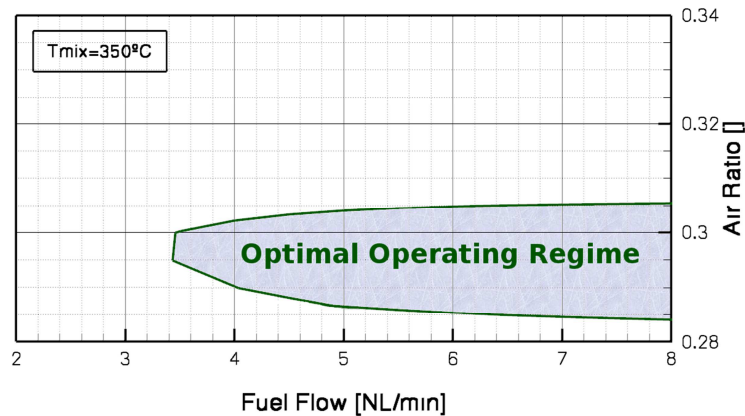

Figure 6 – Range of operating conditions that maximize reformer efficiency and fuel conversion for the actual reactor disposal.

5.2.2 Adiabatic reactor

An adiabatic reactor is now considered by adding to the actual reactor disposal (Figure 1) a catalytic inert front heat shield (FHS), with a length of 2.0 cm, in order to avoid heat losses by radiation from the glowing entrance section of the catalytic monolith. The FHS is assumed to have the same geometrical properties of the catalytic monolith (Table 1) and a perfect continuity between both structures is assumed. Therefore, regarding the mathematical model, instead of Danckwerts type of boundary conditions applied on both gas phase balances, Dirichlet boundary conditions were applied and for energy balance of solid phase a Neumann type of boundary conditions were considered.

Since radiative heat losses, from the inlet section of the catalytic monolith, is by far the most important phenomenon for the observed variation on fuel conversion and reformer efficiency with fuel flow rate variations, in this section it is intended to determine how more efficient would be the reforming process if an adiabatic reactor was applied. Therefore, it is expected a larger domain than the previous (Figure 6) which return, at outlet reformer conditions, the same optimal range for fuel conversion and reformer efficiency.

Thus, Figure 7 shows, for each inlet reformer temperature, isolines of the maximum allowed surface temperature, fuel conversion equal to 98% (for an inlet temperature of 350ºC all domain has a fuel conversion above 98%) and reformer efficiency equal to 87% (for 250ºC and 300ºC) and equal to 88% (for 350ºC). Comparing Figures 5 and 7, one arrives to the conclusion that for each inlet reformer temperature the domain for the same level of reformer efficiency and fuel conversion is higher for an adiabatic reactor.

In Figure 8, the operating regime which assures the same criteria (expression (9)) as that defined in Figure 6, shows that the range for operating conditions are now larger and better, it does not present sensitivity to the input power which is beneficial when it is intended to attain specific throughputs from the reactor without any expense on fuel conversion or reformer efficiency. Figure 8 also shows, through a dashed red line, the maximum achieved reformer efficiency (~89.3%).
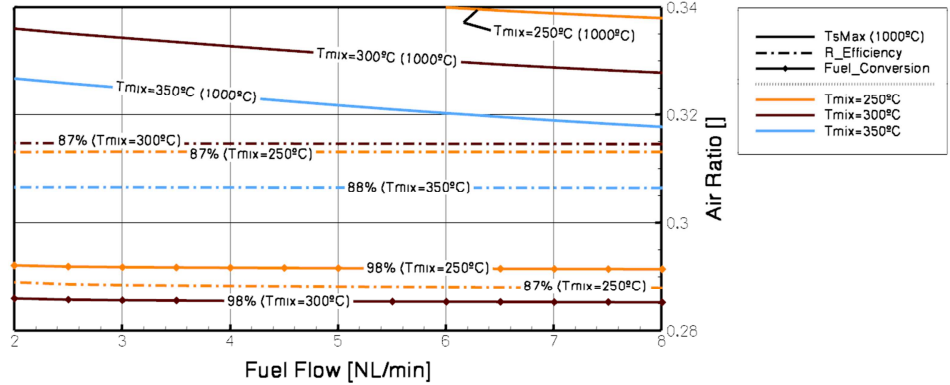

Figure 7 – Isolines of fuel conversion, reformer efficiency and maximum allowable surface temperature for an adiabatic reactor.
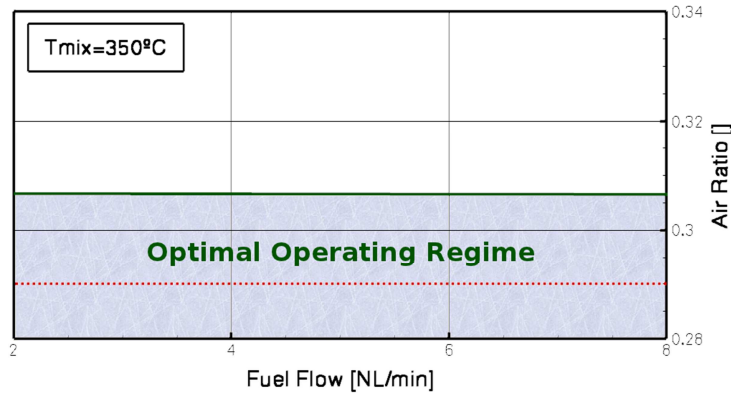

Figure 8 – Range of operating conditions that maximize reformer efficiency and fuel conversion for an adiabatic reactor.

6   CONCLUSIONS

The present work deals with numerical modeling analysis of catalytic partial oxidation of methane in extruded monolith structures coated with PGMs catalysts. The model applied takes into account the coupling between heat and mass transfer and surface chemistry as well as diffusional limitations of mass along washcoat layer. The model was validated for a large set of experimental data.

An optimization procedure was then carried out to define a range for operating conditions which returns at the outlet section of the reactor a specific range for fuel conversion and reformer efficiency while keeping catalyst surface temperatures bellow the maximum value allowed. The optimization procedure was performed for two case studies: 1) with actual nonadiabatic reactor configuration and 2) with an adiabatic reactor. The results for case 1) show that higher levels of fuel conversion and reformer efficiency are observed for higher fuel flow rates since the relative heat losses decrease. For case 2) higher values for fuel conversion and reformer efficiency are noticed comparing with case 1) and these values do not present great sensibility to the input power. However, it is worth noting that the adiabatic case study involves higher overall pressure drop which can be a key parameter in reactor design.

ACKNOWLEDGMENTS

NOMENCLATURE

a_V Specific surface area. $[m^{-1}]$

u Mean flow velocity. $[m.s^{-1}]$

$K_{mat.K}$ External mass transport coefficient. $[m.s^{-1}]$

Y_K Mass fraction of the kth species. [-]

ΔH°_R Enthalpy of reaction at STP conditions. $[J.mol^{-1}]$

V_K Diffusion velocity of the kth species. $[m.s^{-1}]$

C_p Specific heat. $[J.kg^{-1}.K^{-1}]$

h External heat transport coefficient. $[W.m^{-2}.K^{-1}]$

k Thermal conductivity. $[W.m^{-1}.K^{-1}]$

q_R Rate of progress of reaction R. $[mol.kg_{cat}^{-1}.s^{-1}]$

C Molar concentration. $[mol.m^{-3}]$

$D_{eff,k}$ Effective diffusivity of the kth species $[m^2.s^{-1}]$

X_{fuel} Fuel conversion. [-]

d_h Hydraulic channel diameter $[m]$

Greek Letters

ε Bed porosity. [-]

ρ Density. $[kg.m^{-3}]$

ξ Catalytic volumetric fraction. [-]

$v_{k,R}$ Stoichiometric coefficient of species k in reaction R. [-]

$\phi_{k,R}$ Generalized Thiele modulus of reaction R. [-]

η_R Effectiveness factor applied to reaction R. [-]

δ_{cat} Washcoat thickness. $[m]$

ε_s Solid emissivity. [-]

σ Stefan-Boltzmann constant. $[W.m^{-2}.K^{-4}]$

η_{Ref} Reformer Efficiency. [-]

λ Air ratio. Defined according to the stoichiometry of methane total combustion reaction. [-]

Subscripts

s Solid.

g Gaseous mixture.

k,g kth species of gas phase mixture.

k,w kth species of solid phase mixture

cat Catalyst, washcoat.

Superscripts

S External washcoat surface.

eq Chemical equilibrium.

Acronyms

CPOX   Catalytic Partial Oxidation.

CHP   Combined Heat and Power.

SOFC   Solid Oxide Fuel Cell.

PGMs   Platinum Group Metals.

LH   Langmuir-Hinshelwood.

REFERENCES

1. D. A. Hickman and L. D. Schmidt, Synthesis gas formation by direct oxidation of methane over Pt monoliths, *Journal of Catalysis*, 138:267-282, 1992.

2. D. A. Hickman, E. A. Haupfear and L. D. Schmidt, Synthesis gas-formation by direct oxidation of methane over Rh monoliths, *Catalysis Letters*, 17:223-227, 1993.

3. H. Liander, The utilization of natural gases for the ammonia process, *Transactions of the Faraday Society*, 25:462-472, 1929.

4. C. Padovani and P. Franchetti, Giorn. Chem. Ind. Applicatta Catal., 15:429, 1933.

5. M. Prettre, C. H. Eichner and M. Perrin, Catalytic oxidation of methane to carbon monoxide and hydrogen, *Transactions of the Faraday Society*, 43:335-340, 1946.

6. A. P. E. York, T. Xiao and M. L. H. Green, Brief overview of the partial oxidation of methane to synthesis gas, *Topics in Catalysis*, 22:345-358, 2003

7. K. A. Williams, R. Horn and L. D. Schmidt, Performance of mechanisms and reactor models for methane oxidation on Rh, *AIChe Journal*, 53(8):2097-2113, 2007.

8. G. Groppi, A. Beretta and E. Tronconi, *Structured Catalysis and Reactors*, Chapter 8: Monolithic catalysis for gas-phase syntheses of chemicals, 243-310, CRC Press 2006.

9. G. Pepermans, J. Driesen, D. Haeseldonckx, R. Belmans and W. D'haeseleer, Distributed generation: definition, benefits and issues, Energy Policy, 33:787-798, 2005.

10. R. O'Hayre, S-W. Cha, W. Colella and F. B. Prinz, *Fuel Cell Fundamentals*, John Wiley and Sons, New Jersey, 2006.

11. A. Hawkes and M. Leach, Solid oxide fuel cell systems for residential micro-combined heat and power in the UK: key economic drivers, *Journal of Power Sources*, 149:72-83, 2005.

12. I. Frenzel – TU Bergakademie Freiberg, Internal FC-District Communication, D3.1.3, Annex 1, 2011

13. R. Schwiedernoch, S. Tischer, C. Correa and O. Deutschmann, Experimental and numerical study on the transient behavior of partial oxidation of methane in a catalytic monolith, *Chemical Engineering Science*, 58:633-642, 2003.

14. G. Vesser and J. Frauhammer, Modelling steady state and ignition during catalytic methane oxidation in a monolith reactor, *Chemical Engineering Science*, 55:2271-2286, 2000.

15. A. Beretta, A. Donazzi, D. Livio, M. Maestri, G. Groppi, E. Tronconi and P. Forzatti, Optimal design of CH_4 CPO-reformer with honeycomb catalyst: combined effect of catalyst load and channel size on the surface temperature profile, *Catalysis Today*, 171:79-83, 2011.

16. O. Deutschmann and L. Schmidt, Modelling the partial oxidation of methane in a short-contact-time reactor, *AIChe Journal*, 44:2465-2477, 1998.

17. J. Slaa, R. Berger, G. Marin, Partial oxidation of methane to synthesis gas over $Rh/\alpha - Al_2O_3$ at high temperatures, *Catalysis Letters*, 43:63-70, 1997.

18. M. Hartmann, L. Maier, H. D. Minh and O. Deutschmann, Catalytic partial oxidation of iso-octane over rhodium catalysts: an experimental, modeling, and simulation study, *Combustion and Flame*, 157:1771-1782, 2010.

19. L. Maier, M. Hartmann, S. Tischer and O. Deutschmann, Interaction of heterogeneous and homogeneous kinetics with mass and heat transfer in catalytic reforming of logistic fuels, *Combustion and Flame*, 158:796-808, 2011.

20. A. Donazzi, D. Livio, M. Maestri, A. Beretta, G. Groppi, E. Tronconi and P. Forzatti, Synergy of homogeneous and heterogeneous chemistry probed by in situ spatially resolved measurements of temperature and composition, *Angewandte Chemie - Int. Edition*, 50:3943-3946, 2011.

21. D. Livio, A. Donazzi, A. Beretta, G. Groppi and P. Forzatti, Experimental and modeling analysis of the thermal behavior of an autothermal C_3H_8 catalytic partial oxidation reformer, *Industrial & Engineering Chemistry Research*, doi:10.1021/ie2012098q, 2011.

22. A. Beretta, G. Groppi, M. Lualdi, I. Tavazzi and P. Forzatti, Experimental and modeling analysis of methane partial oxidation: transient and steady-state behavior of Rh-coated monoliths, *Industrial & Engineering Chemistry Research*, 48:3825-3836, 2009.

23. A. Donazzi, A. Beretta, G. Groppi, P. Forzatti, Catalytic partial oxidation of methane over a 4% $Rh/\alpha - Al_2O_3$ catalyst. Part I: Kinetic study in annular reactor, *Journal of Catalysis*, 255:241-258, 2008.

24. R. Shah and A. London, *Laminar flow forced convection in ducts*, Academic Press, 1978.

25. G. Froment and K. Bischoff, *Chemical Reactor Analysis and Design*, Wiley, 1990.

26. J. E. P. Navalho, M. A. A. Mendes, J. M. C. Pereira and J. C. F. Pereira, Análise em regime estacionário da oxidação parcial catalítica de metano em Ródio, *Proc. X Congresso Ibero-Americano em Engenharia Mecânica*, pp. 887-898, Porto, 4-7 September 2011.

27. R. C. Reid, J. M. Prausnitz and B. E. Poling, *The Properties of Gases & Liquids*, McGraw-Hill, New York, 1987.

28. R. J. Kee, J. F. Grcar, M. D. Smooke and J. A. Miller, Premix: a Fortran program for modeling steady laminar one-dimensional premixed flames, *Sandia National Laboratories*, Report SAND85-8240, 1985.

29. J. F. Grcar, The twopnt program for boundary value problems, *Sandia National Laboratories*, Report SAND91-8230, 1992.

30. R. J. Kee, F. M. Rubley and E. Meeks, Chemkin-II: a Fortran chemical kinetic package for the analysis of gas-phase chemical kinetics, *Sandia National Laboratories*, Report SAND89-8009, 1989.

31. R. J. Kee, G. Dixon-Lewis, J. Warnatz, M.E. Coltrin and J.A. Miller. A Fortran computer code package for the evaluation of the gas-phase multicomponent transport properties, *Sandia National Laboratories*, Report SAND86-8246, 1986.

32. G. Smith, D. Golden, M. Frenklach, N. Moriarty, B. Eiteneer, M. Goldenberg, C. Bowman, R. Hanson, S. Song, W. Gardiner, Jr., V. Lissianski, Z. Qin, http://www.me.berkeley.edu/gri_mech/.

33. S. Ding, Y. Yang, Y. Jin and Y. Cheng, Catalyst deactivation of Rh-coated foam monolith for catalytic partial oxidation of methane, *Industrial & Engineering Chemistry Research*, 48:2878-2885, 2009.

34. D. D. Nogare, S. Salemi, P. Biasi and P. Canu, Taking advantage of hysteresis in methane partial oxidation over Pt on honeycomb monolith, *Chemical Engineering Science*, 66(24):6341-6349, 2011.